ADVANCED MATERIALS
www.advmat.de

Construction of Six-Oxygen-Coordinated Single Ni Sites on g-C_3N_4 with Boron-Oxo Species for Photocatalytic Water-Activation-Induced CO_2 Reduction

Yuying Wang, Yang Qu, Binhong Qu, Linlu Bai, Yang Liu, Zhao-Di Yang, Wei Zhang, Liqiang Jing,* and Honggang Fu**

The configuration regulation of single-atom photocatalysts (SAPCs) can significantly influence the interfacial charge transfer and subsequent catalytic process. The construction of conventional SAPCs for aqueous CO_2 reduction is mainly devoted toward favorable activation and photoreduction of CO_2, however, the role of water is frequently neglected. In this work, single Ni atoms are successfully anchored by boron-oxo species on g-C_3N_4 nanosheets through a facile ion-exchange method. The dative interaction between the B atom and the sp^2 N atom of g-C_3N_4 guarantees the high dispersion of boron-oxo species, where O atoms coordinate with single Ni (II) sites to obtain a unique six-oxygen-coordinated configuration. The optimized single-atom Ni photocatalyst, rivaling Pt-modified g-C_3N_4 nanosheets, provides excellent CO_2 reduction rate with CO and CH_4 as products. Quasi-in-situ X-ray photoelectron spectra, transient absorption spectra, isotopic labeling, and in situ Fourier transform infrared spectra reveal that as-fabricated six-oxygen-coordinated single Ni (II) sites can effectively capture the photoelectrons of CN along the B—O bridges and preferentially activate adsorbed water to produce H atoms to eventually induce a hydrogen-assisted CO_2 reduction. This work diversifies the synthetic strategies for single-atom catalysts and provides insight on correlation between the single-atom configuration and reaction pathway.

1. Introduction

Catalytic transformations of CO_2 to fuels and chemical feedstocks contribute to managing the global carbon balance so as to alleviate the rapid consumption of fossil resources and growing emission of CO_2.[1,2] Photocatalysis has provided a "green" approach for the transformation of CO_2 by utilizing abundant and sustainable solar energy.[3–5] Hence, tremendous efforts have been made to develop photocatalyst materials for efficient CO_2 reduction reaction (CO_2RR) meanwhile to deepen the recognition on the process mechanism.[6] Among various semiconductors explored as the photocatalyst candidates, the polymeric organic carbon nitride (g-C_3N_4, CN) with visible-light response and robust nature has acquired vast interests.[7] To fabricate ultrathin 2D CN can enlarge the specific surface area, and more importantly inhibit the bulk recombination possibility of charge carriers owning to shortened diffusion distance.[8] Nevertheless, the intrinsic poor charge separation rate and lack of catalytic sites for 2D CN still limit sufficient utilization of the charge carriers to trigger the CO_2 reduction. One of the most comprehensively adopted strategies is to introduce Pt, Au, Ni and Co, etc., based metal/metal complex nanoparticles as cocatalysts onto the CN surface, which can improve the charge separation by capturing the charge carriers and also endow active catalytic sites for CO_2 activation.[3,6,9]

Recently, the focus of metal-based cocatalysts turns to single-atom catalysts (SACs) with the maximum atom efficiency, which demonstrate excellent catalytic activities owing to unique electronic properties of single-atom active sites.[9–12] For the photocatalysts containing single-atom sites as-called single-atom photocatalysts (SAPCs), on one aspect they might capture the charge carriers with much shortened charge transfer distance compared with the metal/metal complex nanoparticles, hence facilitate the charge kinetics of semiconductor supports. On another aspect, the unique electronic structures of the single atoms could significantly influence the metal–support interaction, thus modulating the interfacial charger transfer

Y. Wang, Y. Qu, B. Qu, L. Bai, Y. Liu, L. Jing, H. Fu
Key Laboratory of Functional Inorganic Materials Chemistry (Ministry of Education)
School of Chemistry and Materials Science
Heilongjiang University
Harbin, Heilongjiang 150080, China
E-mail: llbai@hlju.edu.cn; jinglq@hlju.edu.cn; fuhg@vip.sina.com
Z.-D. Yang
School of Materials Science and Chemical Engineering
Harbin University of Science and Technology
Harbin, Heilongjiang 150080, China
W. Zhang
Chongqing Institute of Green and Intelligent Technology
Chinese Academy of Sciences
Chongqing 400714, China
The ORCID identification number(s) for the author(s) of this article can be found under https://doi.org/10.1002/adma.202105482.

DOI: 10.1002/adma.202105482

behavior to further improve charge separation.[13] More importantly, compared with metal/metal complex nanoparticles single metal sites counterpart for extraordinary activities because their capability in tuning the binding strength with reaction intermediates can alter or boost desired photocatalytic pathways.[10–12] Therefore, to rationally fabricate CN-based SAPCs especially precisely control the geometric and electronic structure of single metal sites is promising to realize high-efficiency photocatalytic CO_2RR.

In terms of the structure of CN, there exist abundant periodically separated N atoms, which lone-pair electrons can be utilized for binding the single metal atoms with empty orbitals, hence could potentially provide anchoring sites. Accordingly, atomically dispersed noble and transition metals with N (or C) as coordinating atoms have been successfully constructed on CN.[14–17] As noticed, the catalytic function of single-atom sites for CN-based SAPCs all focus on activating the CO_2 molecules which are difficult to be reduced due to extremely stable C=O bonds. Meanwhile, the activation of water molecules by the single metal sites during the aqueous CO_2RR process is unfavored because it might lead to the H_2 evolution reaction (HER) as a competitive reaction for CO_2RR. However, as the development of the investigation on the process mechanism for CO_2RR in the aqueous environment, the recognition on the role of water is being renewed. Water, both dissociated on the surface of the photocatalyst and in subsequent molecular layers might function as the electron donor reacting with photogenerated holes.[18,19] Besides, they were also found capable of stabilizing the charge carriers to prevent the electron–hole recombination. Noticeably, water can accept photoelectrons to form H atoms as to anticipate the CO_2 reduction process.[18,19] This naturally triggers the association on the catalytic water–gas reaction and CO_2 hydrogenation processes, in which occasions it is proposed that H atoms can impinge adsorbed CO_2 to form the carboxyl intermediates then to initiate the CO_2 reduction.[20] Analogously, to produce H atoms via efficient water activation and photoreduction over specific photocatalysts as a thermodynamically favored process might possibly induce the formation of carboxyl intermediates hence realize the photocatalytic CO_2 reduction by a distinct pathway. To realize as-proposed photocatalytic water-activation-induced CO_2RR definitely requires the SAPC with unique electronic structure that can dominate efficient water activation instead of activating CO_2. In additionally, the single sites of as-designed SAPC are obliged to maintain sparse to inhibit HER.

Inspired by the classical Ni oxides/hydroxides-based typical oxygen evolution reaction (OER) cocatalysts with favorable affinity with water, O atom-anchored single Ni sites are promising to induce preferential adsorption of water.[21,22] Moreover, compared with N and C as the coordination atoms, the O atom with larger electronegativity might result in much facilitated photoelectron transfer between CN support and intended single sites. Next, the challenge lies in that how to fabricate durable O-coordinated single Ni sites on the CN surface. In our previous works, inorganic acids such as phosphate and boric acid were applied to modify the semiconductor surfaces. As-formed phosphorus-oxo and boron-oxo species have been proved to function as "bridge" to facilitate the photoelectron transfer of semiconductor supports.[23] Noteworthily, the B atom of boric acid with less valence electron number than its valence orbital number possesses electron-deficient structure, whereas the sp^2 N atom of CN could function as Lewis base. Thus, it is natural to infer the dative interaction between B and sp^2 N atoms might exist to assist the high dispersion of boron-oxo species on CN.[24] Additionally, we notice the transition metal (TM) cations were reported tending to incorporate with borate to form TM-oxo-borate clusters when dissolved TM salts interact with B_2O_3 or boric acid.[25] This phenomenon hints the boron-oxo species might possibly anchor the single Ni sites with O as the coordination atoms and facilitate the photoelectron transfer from CN to the Ni sites atoms along the B–O bridge under illumination. Based on above consideration, in this work six-oxygen-coordinated single Ni (II) sites were anchored by the highly dispersed boron-oxo species supported on CN naosheets through a facile ion-exchange method. Specifically, highly dispersed boron-oxo species were controllably loaded by the dative interaction between B and sp^2 N atoms with the aid of dehydration between hydroxyl groups, the O atoms of which dominated the anchoring of single Ni (II) sites to acquire a unique six-oxygen-coordinated configuration. It is evidenced by the quasi-in-situ X-ray photoelectron spectra, transient absorption spectra, isotopic labeling, and in situ Fourier transform infrared spectroscopy that under illumination as-fabricated single Ni (II) sites would capture the photoelectrons of CN then preferentially reduce adsorbed water to produce H atoms eventually to induce a unique hydrogen-assisted CO_2 reduction. This work has opened up an in-depth recognition of the structure–performance relationship of SAPC for solar-fuel production.

2. Results and Discussion

2.1. Synthesis and Structural Analysis of Single-Atom Ni-OB-CN Photocatalyst

As shown in **Scheme 1**, pristine CN nanosheets were synthesized by pyrolyzing urea as the raw material, which solid product was then exfoliated by the post-treatment with nitric acid solution to obtain ultrathin CN nanosheets denoted as CN for short. Next, resultant CN was bathed in the aqueous boric acid solution of desired concentration for sufficient interaction. The liquid mixture was then transferred to Teflon for the hydrothermal treatment at 120 °C to result in the boron-oxo species modified CN (OB-CN) samples. Subsequently, by introducing $NiNO_3$ solution dropwise into the aqueous OB-CN suspension, the mixture was gradually evaporated to finally acquire the Ni-modified OB-CN (Ni-OB-CN) photocatalysts. The X-ray diffraction patterns confirm the diffraction peak at 27.3° is assigned to the (002) plane of CN (Figure S1a, Supporting Information).[8] For 5OB-CN and 0.7Ni-5OB-CN, no extra diffraction peaks could be observed, implying no boron or Ni oxide are formed. The diffuse reflection spectra (DRS) indicate both steps of modification for CN do not influence its light absorption (Figure S1b, Supporting Information). The morphology of CN was verified by the transmission electron microscope (TEM). It could be observed that CN takes on 2D and smooth nanosheets (Figure S1c, Supporting Information), For 5OB-CN and 0.7Ni-5OB-CN, neither boron-oxo nor Ni aggregates can be observed on the CN

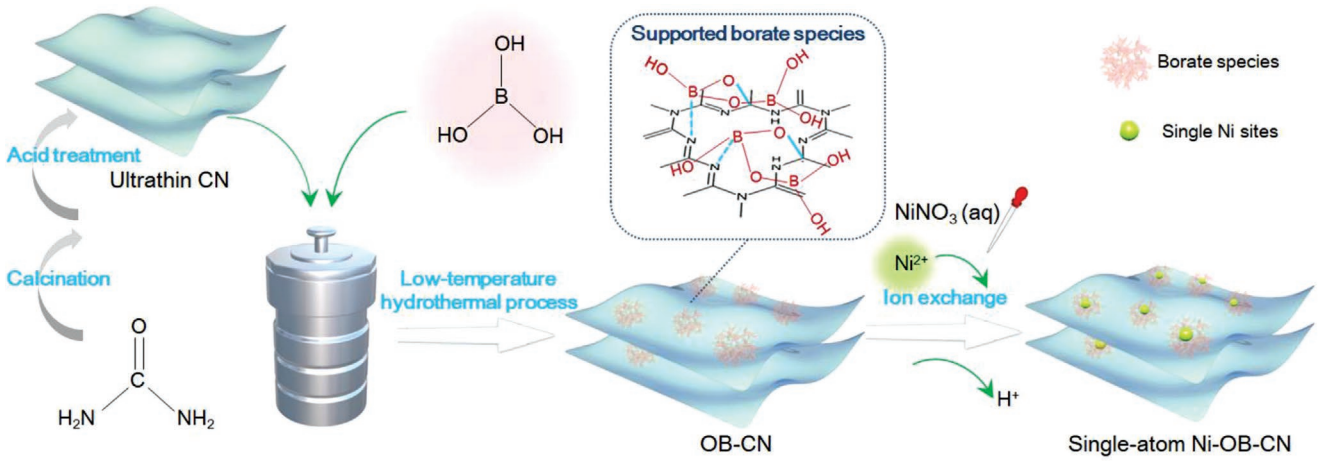

Scheme 1. Synthetic procedures of single-atom Ni (II) sites supported on boric acid-modified carbon nitride nanosheets.

nanosheets in corresponding TEM images (Figure S1d–h, Supporting Information). The average thickness of CN is ≈3 nm as indicated by corresponding atomic force microscope image as shown in Figure S1i in the Supporting Information, which has been basically maintained for 5OB-CN and 0.7Ni-5OB-CN. Above indicates ultrasmall scale of Ni species as well as boron-oxo has been successfully constructed on the surface of CN. The energy-dispersive X-ray spectroscopy mapping of 0.7Ni-5OB-CN evidenced the successful loading of borate and Ni species with uniform distribution (Figure S1l,m, Supporting Information). Furthermore, the exact distribution of Ni species was affirmed by the atomic-resolution high-angle-annular-dark-field scanning transmission electron microscopy (HAADF-STEM). The isolated bright dots are unambiguously assigned to individual Ni atoms, clearly identifying the atomic dispersion of Ni sites as-anchored on the OB-CN (**Figure 1**a and Figure S2,

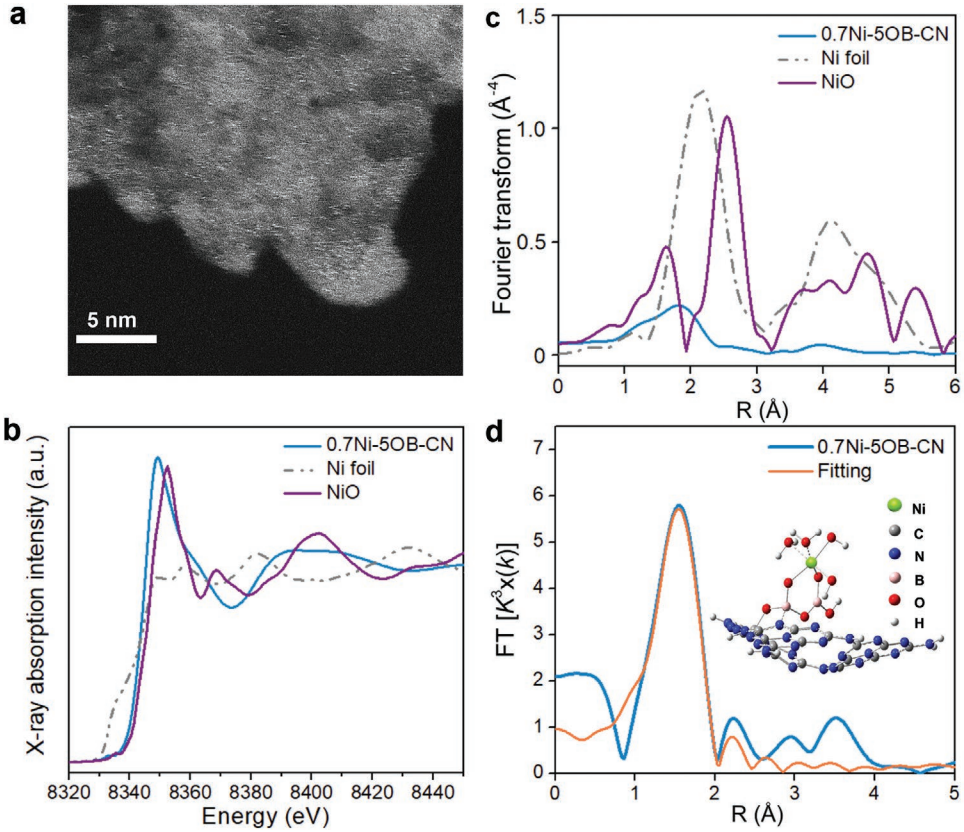

Figure 1. a) The HAADF-STEM image of 0.7Ni-5OB-CN. b) Normalized XANES spectra of 0.7Ni-5OB-CN, NiO, and Ni foil, respectively, at the Ni K-edge. c) Fourier transformation of EXAFS spectra at the Ni K-edge. d) The corresponding EXAFS fitting curves and simulated structure model of hydrated single-atom Ni-OB-CN photocatalyst as the inset.

Supporting Information). The chemical composition and elemental states of CN, 5OB-CN, and 0.7Ni-5OB-CN were investigated by the X-ray photoelectron spectroscopy (XPS). The Ni $2p_{3/2}$ peak at 855.2 eV is attributed to the oxidative Ni^{2+} species of 0.7Ni-5OB-CN (Figure S3a, Supporting Information).[26–29] The identical peaks at 191.5 eV for 5OB-CN and 0.7Ni-5OB-CN are ascribed to the oxidative boron (Figure S3b, Supporting Information).[23] It is noted that the O 1s peak for 0.7Ni-5OB-CN shifts to higher binding energy compared with that for 5OB-CN mainly due to more absorbed water molecules on Ni sites (Figure S3c, Supporting Information). Moreover, as indicated in Figure S3d in the Supporting Information compared with CN, the C—O component ratios for 5OB-CN and 0.7Ni-5OB-CN obviously increase, which originates from the dehydration when loading borate species on CN surface. For the N 1s spectra of three typical samples, the deconvoluted peaks are assigned to N=C—N, CN_3, and NH_x, respectively. No additional N 1s peaks appear, implying no direct N-involved chemical bonds are formed as the loading of boron-oxo or single Ni species (Figure S3e, Supporting Information). The oxidation state of the single Ni atoms were further determined from the position of the rising edge of the Ni K-edge X-ray absorption near edge structure (XANES) spectra, in comparison with NiO and Ni foil (Figure 1b). The spectral line shape and the absorption edge position closely resemble those of NiO, indicating the oxidation state of the Ni single atoms is close to +2, which agrees well with the Ni 2p XPS results.[27–29] Figure 1c displays the Fourier transform of the extended X-ray absorption fine structure (EXAFS) spectra. There is no first-shell Ni–Ni contribution for 0.7Ni-5OB-CN, suggesting that Ni species are not in the form of metallic Ni nanoparticles or clusters. Corresponding with the HAADF-STEM result, it is affirmed single-atom Ni species are successfully loaded on 5OB-CN. The EXAFS data fitting results are shown in Figure 1d, Figure S4, and Table S1 in the Supporting Information. The main peak at ≈1.53 Å is attributed to the scattering interaction between the Ni atoms and the first shell (Ni—O), and the coordination number is approximately six. It is noted the Ni-O bond length of as-constructed Ni atoms is similar as that of NiO contrast. On account of above analysis, it is evidenced that supported highly dispersed boron-oxo species anchor single Ni sites by the O atoms. Therefore, it could be deduced that high dispersion of boron-oxo species on CN surface is the key of realizing the atomic dispersion of Ni (II) species. Generally, boric acid would easily be dehydrated intermolecularly and with the hydroxyl groups of supports then form boron oxide nanoparticles under thermo-treatment, however which are negligible for OB-CN. This implies that there might exist unique interfacial interaction between boron-oxo species and the CN support. Considering the electron-deficient structure of B atoms while the sp^2 N of CN as Lewis base, it is inferred that the high dispersion of boron-oxo species might be attributed to the dative interaction between B and sp^2 N atoms. To verify the postulate, the solid ^{15}N NMR spectra were collected to uncover the interaction between boron-oxo clusters and CN (Figure S5, Supporting Information). For ^{15}N-labeled pristine CN, the signal at 202 ppm was attributed to the sp^2 N atoms directly connected to C atoms while the ones at 145 and 116 ppm corresponded to the secondary bridging amine (NH).[30] After introducing boron-oxo species, it is noticeable that the peak at 202 ppm shifts to downfield, indicating the chemical environment change of sp^2 N atoms was highly possibly induced by a dative interaction instead of chemical bonding. Combining all acquired structure information, simplified structure models of CN and OB-CN were simulated by the density functional theory (DFT) calculation with the metaboric acid as a basic boron-oxo unit (Figure S6a and b, Supporting Information). Accordingly, the pristine and hydrated model of single-atom Ni-OB-CN photocatalyst was obtained as Figure S6c in the Supporting Information and Figure 1d inset, respectively. It is confirmed that the O atoms of supported boron-oxo species anchor single Ni^{2+} atoms, meanwhile with the assistance of the O atoms of hydroxyl groups and water molecules, to eventually result in single six-oxygen-coordinated Ni (II) sites (Ni (II)-O_6).

2.2. Photocatalytic Performances for CO_2RR and Charge Separation Properties

The photoactivities of as-fabricated samples for CO_2RR were examined under the UV-vis light irradiation without any sacrificial reagents. By altering the using amount of boric acid, the best performance for boric acid-modified CN was obtained for 5OB-CN (Figure S7a, Supporting Information). On the basis of 5OB-CN, the amount of Ni species introduced was further optimized as Figure S7b in the Supporting Information. In a result, 0.7Ni-5OB-CN shows the best photoactivity with the CO and CH_4 production rates of 22.1 and 8.7 μmol g^{-1} h^{-1}, respectively. Moreover, the CO_2 conversion rate of 0.7Ni-5OB-CN achieves around 10 and 35 times of that for CN and bulk CN, respectively (**Figure 2**a). Noteworthily, 0.7Ni-5OB-CN is advantageous over 0.7Ni-CN and surprisingly rivals 0.7Pt-CN as the contrast samples containing the same moles of metal species. To avoid misleading information because inevitable organic impurities in carbon-based catalysts can possibly be oxidized to hydrocarbons (e.g., methanol or other organic products), the photoreduction of ^{13}C-labeled CO_2 was conducted over the 0.7Ni-5OB-CN photocatalyst. Dominant peak of ^{13}CO ($m/z = 29$) and tiny peak of $^{13}CH_4$ ($m/z = 17$) were observed in the selective ion detection chromatography spectrum (Figure S8, Supporting Information). The results verify that evolved C-products originate from the photoreduction of $^{13}CO_2$. Hence, it is concluded that the advantageous electronic structure of single Ni (II)-O_6 sites can well benefit the photocatalytic CO_2 reduction. What cannot be neglected is the photocatalytic HER comprehensively occurring as a competitive reaction for CO_2RR. Remarkably, by the examination of the reduction products over 0.7Ni-5OB-CN no H_2 was evolved, demonstrating the favorable selectivity of single-atom Ni-OB-CN photocatalyst toward CO_2RR. In addition, O_2 was also found evolved as the photo-oxidation product, as inferred related with elevated valance band of CN nanosheets compared with bulk CN.[31] To evaluate the stability of as-fabricated single-atom Ni photocatalyst, five consecutive runs were then carried out over 0.7Ni-5OB-CN photocatalyst (Figure S9, Supporting Information). Within 30 h, the photocatalytic activity of 0.7Ni-5OB-CN for CO_2RR along with its basic morphology and crystalline structure maintained unchanged. Based on above, as-fabricated single-atom Ni-OB-CN photocatalyst

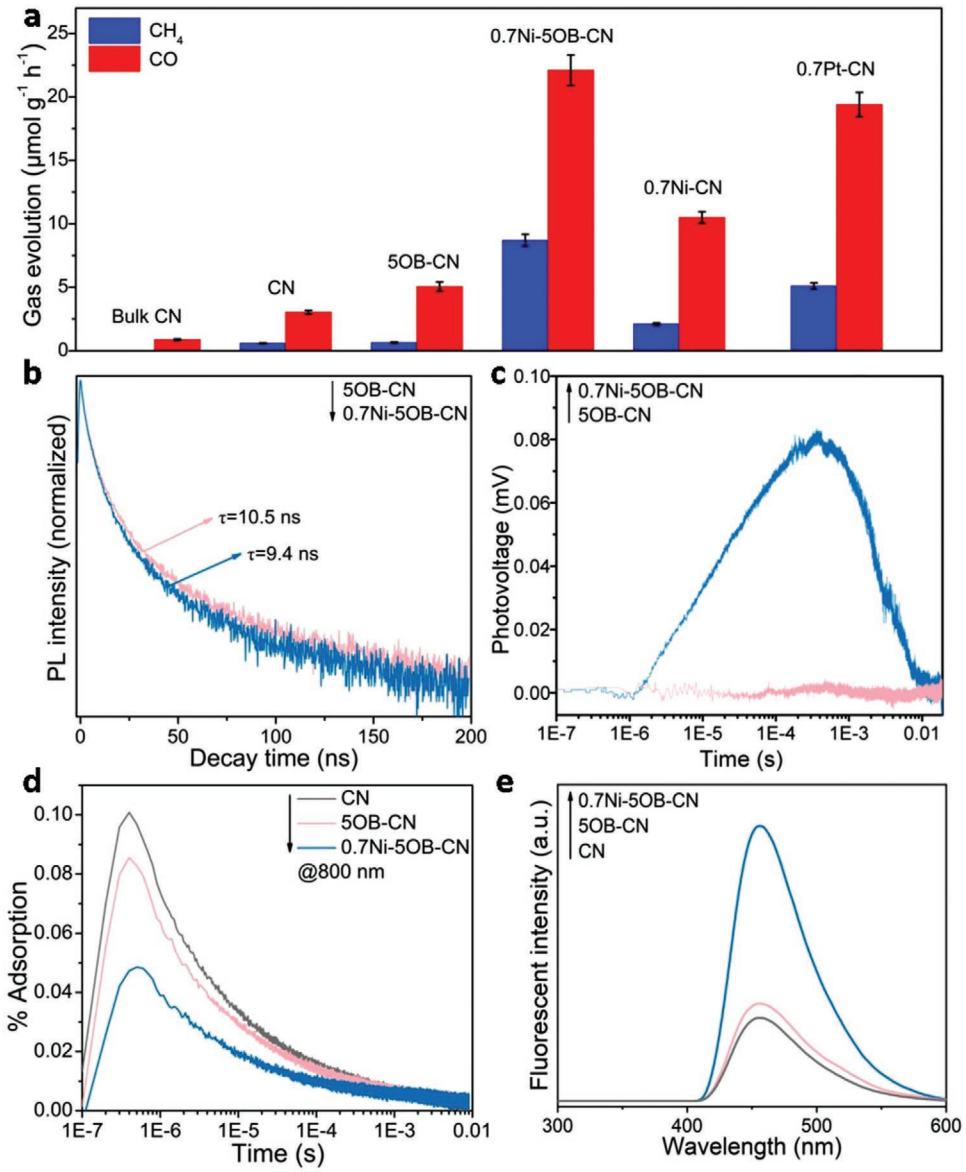

Figure 2. a) Photocatalytic activities of CN, 5OB-CN, and 0.7Ni-5OB-CN for CO_2RR under UV–vis light irradiation. Data are presented as the mean ± standard deviation (SD) from three independent experiments. b) TS-PL spectra and c) TS-SPV spectra in the N_2 atmosphere of 5OB-CN and 0.7Ni-5OB-CN. d) μs-TAS decay kinetics of CN, 5OB-CN, and 0.7Ni-5OB-CN in water monitored at 800 nm and excited by pulsed 355 nm excitation (460 μJ cm^{-2}). e) FS of CN, 5OB-CN, and 0.7Ni-5OB-CN.

exhibits advantageous performance and robust nature in the photocatalytic process of CO_2RR.

Normally, the photocatalytic performance depends on the charge separation of the photocatalyst. The charge transfer behavior between single metal atoms and CN significantly decides the modulating efficiency of photoelectrons.[32–34] To investigate the charge dynamics of as-fabricated single-atom Ni-OB-CN photocatalyst, the transient-state photoluminescence (TS-PL) spectra were collected for typical samples. Figure 2b shows the normalized TS-PL kinetics of CN, 5OB-CN, and 0.7Ni-5OB-CN. The TS-PL decay profiles indicate the decay lifetime of 5OB-CN is decreased from 10.5 to 9.4 ns by introducing single Ni sites, providing an electron transfer efficiency of 10.5%. The shortened PL decays suggest that the electron transfer adds decay channel to the excited states of CN, indicative of quantified charge carrier modulation effect of single Ni sites. To evaluate the photoelectron capture ability of as-constructed single Ni sites objectively, in a benchmark test for CN the $AgNO_3$ solution was introduced as typical electron scavenger. In Figure S10 in the Supporting Information, the decay lifetime with $AgNO_3$ solution added is decreased from 9.8 to 8.3 ns with the electron transfer efficiency of 15.3%. By contrast, the photoelectron capture ability of single Ni sites could rival Ag^+, further affirming its excellent electron capture capacity. Besides, the steady-state surface photovoltage spectroscopy (SS-SPS) signal originates from the surface charge amount change after illumination hence could reflect the photogenerated charge separation status. To elucidate the specific roles of single Ni sites

on charge separation, the SS-SPS responses of all samples were collected by controlling the atmospheres. For CN and 5OB-CN, neglectable response in N_2, different from those in air and O_2, indicates as-introduced boron-oxo species could not capture the photoelectrons (Figure S11a,b, Supporting Information). While the response of 0.7Ni-5OB-CN in N_2 is obvious and corresponding intensities obey the sequence $N_2 < air < O_2$, suggesting single Ni sites can effectively capture the photoelectrons then transfer electrons to adsorbed O_2 (Figure S11c, Supporting Information). Among all Ni-modified samples, 0.7Ni-OB-CN shows the largest SPS signal (Figure S11d, Supporting Information). To further clarify the role of single Ni sites in charge separation, the transientstate surface photovoltage (TS-SPV) responses in N_2 atmosphere proved the modulation effect of single Ni species on photoelectrons (Figure 2c). Compared with 5OB-CN showing no signal, 0.7Ni-5OB-CN exhibits a detectable positive response, confirming the photoelectrons transfer to as-constructed single Ni sites under illumination. Transient absorption spectra (TAS) are a powerful technique to elucidate the charge carrier separation of photocatalysts. Especially, μs-timescale TAS is directly associated with the photocatalytic process subsequent to the charge separation hence could provide information with insight on the charge carriers-induced catalytic processes.[35] Here, we applied μs-TAS to experimentally examine the photoelectron properties of CN, 5OB-CN, and 0.7Ni-5OB-CN mimicking the reaction conditions. As Figure 2d, similar as previous observations on CN-based photocatalysts, the broad photoinduced signal observed at 800 nm is assigned to photogenerated electrons of CN.[34] The TAS spectrum of 5OB-CN resembles that of CN, indicating as-introduced boron-oxo species shows negligible effect on the lifetime of photoelectrons. Differently, 0.7Ni-5OB-CN shows much smaller signal amplitude than CN and 5OB-CN throughout the probed window, inferring electron transfer from CN to the single Ni sites. Briefly, we have identified single-atom Ni species could capture the photoelectrons to enhance the charge separation. Besides, the steady-state photoluminescence (SS-PL) spectra and the fluorescence spectra (FS) related to the produced •OH amount (Figure S12a,b, Supporting Information and Figure 2e) are consistent with above conclusions on the charge separation as well as the photoactivities. Based on above, as-anchored single Ni sites have been evidenced capable of effectively capturing the photoelectrons hence facilitate the charge separation at the CN interface to result in greatly enhanced photocatalytic activities in CO_2RR.

2.3. Molecular Activation and Photocatalytic CO_2RR Mechanism

On the basis of favorable charge separation, subsequent catalytic efficiency is another critical factor that significantly affects the photocatalytic performance. Resembling the Ni oxides/hydroxides catalysts for OER, the saturated single Ni (II)-O_6 sites is predicted to possess good affinity with water. To examine the water adsorption situation, the Fourier transform infrared spectroscopy (FTIR) spectra were collected and are shown in **Figure 3**a, the peaks at around 1600 and 3600 cm^{-1} are related to absorbed water of samples. Here, we utilize the peak height ratio between the two broad peaks to semiquantitatively compare the relative absorbed water content of the samples. Calculated peak height ratios for CN, 5OB-CN, and 0.7Ni-5OB-CN are 0.36, 0.41, and 0.59, respectively, indicating that the loading of boron-oxo species and single-atom Ni sites promote the water affinity of CN in step. Additionally, the H_2O temperature-programmed desorption (TPD)-mass of testing evaporated water was also performed to investigate the interaction between the photocatalysts and water. In the TPD-mass spectra, 0.7Ni-5OB-CN shows the largest water adsorption area and the highest desorption temperature (Figure 3b). To verify the promoted affinity achieved by the modifications with boric acid and single Ni sites, periodic DFT calculations were thus performed to assess the water adsorption energies for typical samples (Figure 3c). For pristine CN, the water molecule would tend to coordinate with the hydroxyl groups on the CN surface, in which situation the adsorption energy was calculated to be −0.12 eV. After the modification of borate species, the adsorption energy is increased to be −0.26 eV. For single Ni photocatalyst, the water adsorption energy of −1.33 eV remarkably surpasses 10 times of that for pristine CN, proving that as-fabricated Ni sites possess excellent water adsorption ability. To further reveal the interaction between 0.7Ni-5OB-CN with water, quasi-in-situ XPS spectra were collected for the pristine 0.7Ni-5OB-CN and partially hydrated 0.7Ni-5OB-CN (0.7Ni-5OB-CN-water) as shown in Figure S13a in the Supporting Information. For the O 1s kinetic spectra (Figure 3d), an obvious shift could be observed, the differential spectrum of O 1s is obtained (Figure S13b in the Supporting Information) by the subtraction of the *Y*-axis values. Next step, according to the equation $E_{binding}$ (O 1s) = $E_{kinetic}$ (C 1s) + $E_{binding}$ (O 1s) − $E_{kinetic}$ (C 1s), the kinetic energy of O 1s was converted to the binding energy to obtain the O 1s spectra in Figure 3e, in which the binding energy of O 1s at 532.0 eV could be found as ascribed to the oxygen of –OH. For the C 1s and N 1s kinetic spectra (Figure S13c,d, Supporting Information), no obvious change could be observed before and after water adsorption. This clearly confirms the significantly promoted water affinity of as-fabricated single Ni sites. By contrast, the affinity of the single-atom Ni-OB-CN photocatalyst was examined by CO_2-TPD-mass spectra. The identical curves for CN, 5OB-CN, and 0.7Ni-5OB-CN in Figure S14 in the Supporting Information evidence neither boron-oxo nor Ni species increase the adsorption with CO_2. Moreover, the calculated adsorption energy of the single Ni photocatalyst toward CO_2 is 1.68 eV (Figure S15, Supporting Information). This hints that the single-atom Ni (II)-O_6 sites could hardly adsorb CO_2 due to its unique six-oxygen-coordinated configuration.

The electrochemical reduction measurements were carried out to further reveal the catalytic ability of the single Ni sites relevant to potential reactants water and CO_2. In the N_2-bubbled system (**Figure 4**a), the water reduction is highly favorable on the 0.7Ni-5OB-CN compared with CN and 5OB-CN, which is due to as-proved water affinity. While in the CO_2-bubbled system, the onset potentials of different CN-based electrodes for water reduction were identical with those of the N_2-bubbled system (Figure 4a, inset), suggesting that the reduction behavior of CO_2 was not preferred for 0.7Ni-5OB-CN. This is because first as verified by above analysis Ni (II)-O_6 sites possess better water affinity and second the reduction of water to produce H atoms is more thermodynamically favored process than the direct reduction of CO_2. Therefore, it is inferred

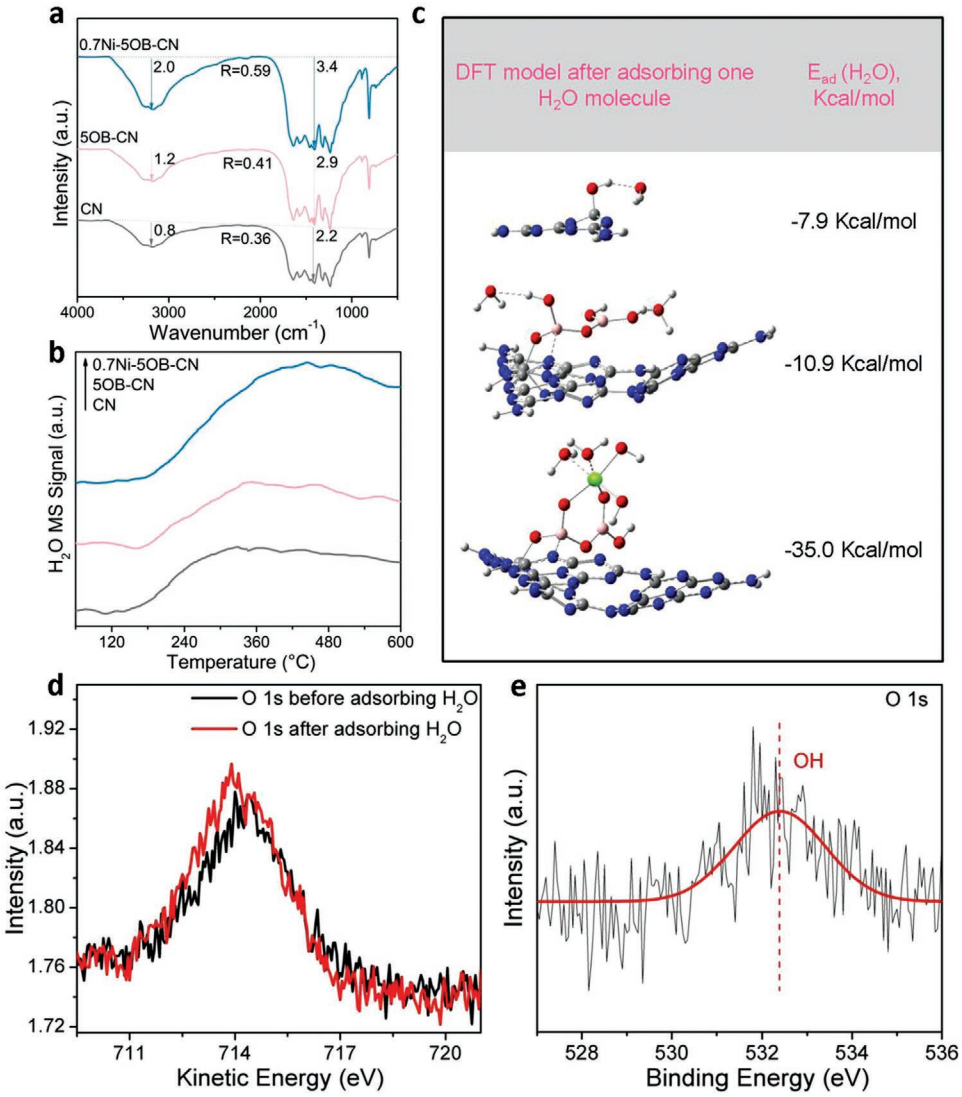

Figure 3. a) FTIR spectra, b) H_2O-TPD-mass spectra, c) water adsorption energies for CN, 5OB-CN, and 0.7Ni-5OB-CN, respectively. d) XPS O 1s spectra of 0.7Ni-5OB-CN before and after water adsorption. e) Differential kinetic energy spectrum of O 1s spectra of 0.7Ni-5OB-CN before and after water adsorption.

that as-produced H atoms from water reduction be the dominant active radicals to induce the reduction of CO_2 analogous to the water–gas reaction process. To provide proves for the inference, the isotopic experiments using D_2O to replace H_2O were employed under identical photocatalytic reaction conditions. For the examination of the gaseous products by the gas chromatography-mass spectrometer (GC-MS) for the photocatalytic system with D_2O as the solvent (Figure S16a, Supporting Information), only ions C (m/z = 12), CD (m/z = 14), CD_2 (m/z = 16), CD_3 (m/z = 18), and CD_4 (m/z = 20) of even m/z were successfully detected, indicating the hydrogen in the produced methane mainly originate from the water. In addition, considering larger bond energy of D—O than H—O, detected CD_4 reflects the excellent water activation ability of as-fabricated 0.7Ni-5OB-CN. In the contrast reaction, a certain amount of CH_3OH was deliberately added to this system with D_2O. It is comprehensively accepted that CH_3OH as the sacrificial agent could capture holes then to facilitate the photocatalytic reaction. Moreover, there exists a controversial recognition that added CH_3OH could provide protons to anticipate the CO_2 reduction process hence reasonably the hydrogen of produced methane might partially originate from CH_3OH. The GC-MS detection (Figure S16b, Supporting Information) demonstrates that similar ions especially no oddly m/z ones could be examined in the CO_2RR products when the CH_3OH was added and 1.7 times CD_4 amount is obtained compared with the experiment without CH_3OH. Although the H/D exchange easily happens, it could still be deduced that for the CO_2RR under 0.7Ni-OB-CN, deuterium is the hydrogen source in produced methane.[36] Interestingly, it is noted that for the photocatalytic CO_2 reduction in H_2O, the introduction of the same amount of CH_3OH leads to ≈1.69 time the moles of CH_4 than the case without CH_3OH as shown in Figure 4b right (relevant GC raw data are shown in Figure S17, Supporting Information). The identical extents of

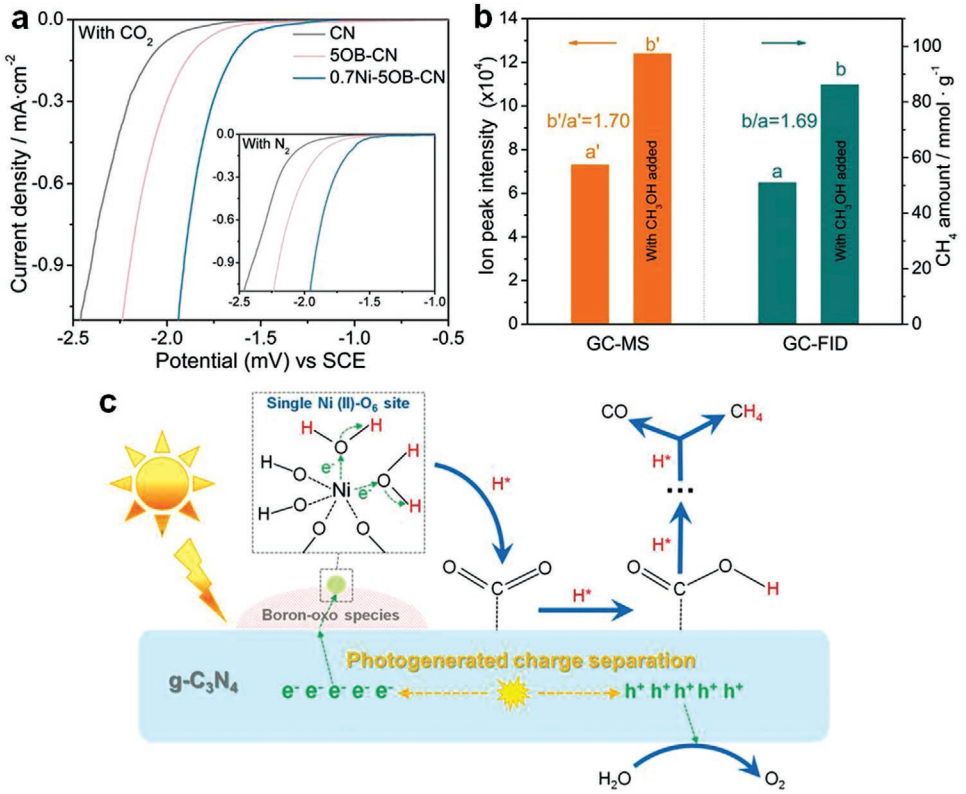

Figure 4. a) Electrochemical reduction curves for CN, 5OB-CN, and 0.7Ni-5OB-CN in CO_2- and N_2-bubbled systems, respectively. b) GC-MS (left) and GC (right) results of 0.7Ni-5OB-CN for detecting produced methane under UV–vis light irradiation. The ion peak intensities of CD_4 in D_2O with and without CH_3OH are denoted as "a" and "b," respectively. The amount of CH_4 evolved in H_2O with and without CH_3OH is denoted as "a" and "b," respectively. c) The possible hydrogen-assisted CO_2 reduction process mechanism over single-atom Ni-OB-CN photocatalyst under illumination.

the photoactivity enhancement with same amount of CH_3OH added hint that the photocatalytic CO_2 reduction in D_2O and H_2O shares similar kinetic processes via preferential water activation. To sum up, the photogenerated electrons would be collected by the six-oxygen-coordinated Ni (II) sites under illumination then preferentially reduce the absorbed water molecules to form H atoms as active species to induce further CO_2 reduction. To acquire an entire picture on the CO_2 reduction process, the in situ FTIR spectra of 0.7Ni-5OB-CN were collected under similar conditions with real photocatalytic reaction (Figure S18, Supporting Information). The band at 1729 cm^{-1} along with the bands in the range of 1700–1900 cm^{-1} is ascribed to the carboxy group in carboxylic acids as inferred belonging to the loosely absorbed carboxyl intermediates such as *COOH.[3,37–39] Therefore, the possible reaction mechanism is summarized in Figure 4c. Under the light irradiation, single Ni (II)-O_6 sites capture the photoelectrons of excited CN nanosheets then reduce the absorbed water molecules to produce H atoms as the active species to further impinge absorbed CO_2 adjacent to the single-atom Ni sites resulting in the carboxyl intermediates, subsequently which are dehydrated by H atoms to form CO*, and finally generate CO and CH_4.

Encouragingly, the boric-acid-mediated strategy of fabricating SAPC is found applicable to typical transition metals Co and Fe. The HAADF-STEM images of 0.7Co-5OB-CN and 0.7Fe-5OB-CN clearly verified the single-atom dispersion of Co and Fe species, respectively (Figure S19a,b, Supporting Information). Similar as the single Ni photocatalyst, as-introduced Co and Fe sites did not change the crystalline structure of CN or the light absorption but significantly improved the charge separation of CN (Figures S20 and 21, Supporting Information). For 0.7Co-5OB-CN, 0.7Fe-5OB-CN, and 0.7Ni-5OB-CN photocatalysts, the CO_2 conversion rates were found in positive correlation with their charge separation (Figure S22, Supporting Information). The above results indicate M-OB-CN might become a novel and universal SAC model.

3. Conclusion

We have successfully developed a novel and universal boric-acid-mediated strategy to construct single transition metal atoms (Ni, Co, and Fe) on CN nanosheets, depending on the uniform distribution of boron-oxo species via dative B–N coordination, as highly active photocatalysts for CO_2 reduction. Under illumination the single Ni sites with saturated coordination by O atoms would effectively capture the photoelectrons then preferentially activate absorbed water molecules to produce H atoms as active species to impinge CO_2 then to ultimately produce CO and CH_4 as products following a distinct hydrogen-assisted CO_2 reduction pathway. This work has evoked a new chapter for the rapid construction of robust single-atom materials and also deepened the understanding on the relationship between electronic structure of single sites and reaction mechanism.

Supporting Information

Supporting Information is available from the Wiley Online Library or from the author.

Acknowledgements

Y.Y.W. and Y.Q. contributed equally to this work. The authors gratefully acknowledge the financial support of NSFC projects (U1805255) and the National Key R&D Program of China (2018YFE0201704). Prof. Baoyu Xia, Huazhong University of Science and Technology and Prof. Jun Xu, Nankai University are acknowledged for generous support.

Conflict of Interest

The authors declare no conflict of interest.

Data Availability Statement

Research data are not shared.

Keywords

g-C_3N_4, photocatalytic CO_2 reduction, photoelectron modulation, single-atom catalysis, water activation

Received: July 15, 2021
Revised: August 24, 2021
Published online: September 27, 2021

[1] M. Aresta, A. Dibenedetto, A. Angelini, *Chem. Rev.* **2014**, *114*, 1709.
[2] Z. Sun, Tao. Ma, H. Tao, Q. Fan, B. Han, *Chem* **2017**, *3*, 560.
[3] A. Li, Q. Cao, G. Zhou, B. V. K. J. Schmidt, W. Zhu, X. Yuan, H. Huo, J. Gong, M. Antonietti, *Angew. Chem., Int. Ed.* **2019**, *58*, 14549.
[4] J. R. Ran, M. Jaroniec, S.-Z. Qiao, *Adv. Mater.* **2018**, *30*, 1704649.
[5] J. Yang, Z. Y. Wang, J. C. Jiang, W. X. Chen, F. Liao, X. Ge, X. Zhou, M, Chen , R. L. Li, Z. G. Xue, G. Wang, X. Z. Duan, G. Q. Zhang, Y. G. Wang, Y. E. Wu, *Nano Energy* **2020**, *76*, 105059.
[6] a) J. Sun, J. Bian, J. Li, Z. Zhang, Z. Li, Y. Qu, L. Bai, Z. D. Yang, L. Jing, *Appl. Catal., B* **2020**, *277*, 119199; b) K. Hu, Z. Li, L. Bai, F. Yang, X. Chu, J. Bian, Z. Zhang, H. Xu, L. Jing, *Sol. RRL* **2020**, *5*, 2000472; c) A. Zada, M. Humayun, F. Raziq, X. Zhang, Y. Qu, L. Bai, C. Qin, L. Jing, H. Fu, *Adv. Energy Mater.* **2016**, *6*, 1601190; d) J. Di, Bo Lin, B. Tang, S. Guo, J. Zhou, Z. Liu, *Small Struct.* **2021**, 2100046, https://doi.org/10.1002/sstr.202100046.
[7] a) S. B. Tian, Q. Fu, W. X. Chen, Q. C. Feng, Z. Chen, J. Zhang, W.-C. Cheong, R. Yu, L. Gu, J. C. Dong, J. Luo, C. Chen, Q. Peng, C. Draxl, D. S. Wang, Y. D. Li, *Nat. Commun.* **2018**, *9*, 2353; b) Y. Wang, P. P. Du, H. Z. Pan, L. Fu, Y. Zhang, J. Chen, Y. W. Du, N. J. Tang, G. Liu, *Adv. Mater.* **2019**, *31*, 1807540; c) Q. H. Liang, Z. Li, Z. H. Huang, F. Y. Kang, Q. H. Yang, *Adv. Funct. Mater.* **2015**, *25*, 6885.
[8] a) Y. Wang, P. Du, H. Pan, L. Fu, Y. Zhang, J. Chen, Y. Du, N. Tang, G. Liu, *Adv. Mater.* **2019**, *31*, 1807540; b) T. Ma, Y. Tang, S. Dai, S. Z. Qiao, *Small* **2014**, *10*, 2382.
[9] a) Y. Zhang, B. Xia, J. Ran, K. Davey, S. Z. Qiao, *Adv. Energy Mater.* **2020**, *10*, 1903879; b) J. Yang, W. Li, D. Wang, Y. Li, *Small Struct.* **2021**, *2*, 2000051.
[10] Y. Q. Zou, S. Y. Wang, *Adv. Sci.* **2021**, *8*, 2003579.
[11] W. P. Ni, Z. X. Liu, Y. Zhang, C. Ma, H. Q. Deng, S. G. Zhang, S. Y. Wang, *Adv. Mater.* **2021**, *33*, 2003238.
[12] W. W. Fu, Y. W. Wang, W. Tian, H. J. Zhang, J. Li, S. Y. Wang, Y. Wang, *Angew. Chem., Int. Ed.* **2020**, *59*, 237911.
[13] a) X. Ge, G. R. Su, W. Che, J. Yang, X, Zhou , Z. Y. Wang, Y. T. Qu, T. Yao, W. Liu, Y, E. Wu , *ACS Catal.* **2020**, *10*, 10468; b) H. Zhao, Y. F. Zhao, J. Gan, J. Xu, Y. Wang, H. W. Lv, S. Fang, Z. Y. Wang, Z. L. Deng, X. Q. Wang, P. G. Liu, W. X. Guo, B. Y. Mao, H. J. Wang, T. Yao, X. Hong, S. Q. Wei, X. Z. Duan, J. Luo, Y, E. Wu , *J. Am. Chem. Soc.* **2020**, *142*, 12643; c) Z. Y. Wang, J. Yang, J. B. Cao, W. X. Chen, G. Wang, F. Xiao, X. Zhou, F. Y. Zhou, R. L. Li, Z. Q. Yu, G. Q. Zhang, X. Z. Duan, Y. E. Wu, *ACS Nano* **2020**, *14*, 6164; d) X. B. Zheng, P. Li, S. X. Dou, W. P. Sun, H. G. Pan, D. S. Wang, Y. D. Li, *Energy Environ. Sci.* **2021**, *14*, 2809.
[14] Y. Li, Z. Wang, T. Xia, H. Ju, K. Zhang, R. Long, Q. Xu, C. Wang, L. Song, J. Zhou, *Adv. Mater.* **2016**, *28*, 6959.
[15] P. Huang, J. Huang, S. A. Pantovich, A. D. Carl, T. G. Fenton, C. A. Caputo, R. L. Grimm, A. I. Frenkel, G. Li, *J. Am. Chem. Soc.* **2018**, *140*, 16042.
[16] C. Tang, L. Chen, H. J. Li, L. Q. Li, Y. Jiao, Y. Zheng, H. L. Xu, K. Davey, S.-Z. Qiao, *J. Am. Chem. Soc.* **2021**, *143*, 7819.
[17] Q. Li, W. T. Bi, L. Zhang, S. Tao, W. S. Chu, Q. Zhang, Y. Luo, C. Z. Wu, Y. Xie, *Adv. Mater.* **2016**, *28*, 2427.
[18] M. Dimitrijevic, B. K. Vijayan, O. G. Poluektov, T. Rajh, A. K. Gray, H. He, P. Zapol, *J. Am. Chem. Soc.* **2011**, *133*, 3964.
[19] W. C. Ma, S. J. Xie, X. G. Zhang, F. F. Sun, J. C. Kang, Z. Jiang, Q. H. Zhang, D. Y. Wu, Y. Wang, *Nat. Commun.* **2019**, *10*, 892.
[20] W. Li, K. M. Stocker, G. C. Schatz, *J. Am. Chem. Soc.* **2017**, *139*, 4663.
[21] K. Sun, F. H. Saadi, M. F. Lichterman, W. G. Hale, H. P. Wang, X. Zhou, N. T. Plymale, S. T. Omelchenko, J. H. He, K. M. Papadantonakis, *Proc. Natl. Acad. Sci. USA* **2015**, *112*, 3612.
[22] O. Diaz-Morales, D. Ferrus-Suspedra, M. Koper, *Chem. Sci.* **2016**, *7*, 2639.
[23] a) Y. Luan, Y. Feng, M. Xie, W. Jing, L. Jing, *RSC Adv.* **2014**, *4*, 29964; b) Z. J. Li, Y. B. Luan, Y. Qu, L. Q. Jing, *ACS Appl. Mater. Interfaces* **2015**, *7*, 22727.
[24] a) R. Nishiyabu, Y. Kubo, T. D. James, J. S. Fossey, *Chem. Commun.* **2011**, *47*, 1124; b) E. Sheepwash, V. Krampl, R. Scopelliti, O. Sereda, A. Neels, K. Severin, *Angew. Chem., Int. Ed.* **2011**, *50*, 3034.
[25] J. T. Rijssenbeek, D. J. Rose, R. C. Haushalter, J. Zubieta, *Angew. Chem., Int. Ed.* **1997**, *36*, 1008.
[26] H. B. Yang, S. F. Hung, S. Liu, K. D. Yuan, S. Miao, L. P. Zhang, X. Huang, H. Wang, W. Z. Cai, R. Chen, J. J. Gao, X. F. Yang, W. Chen, Y. Q. Huang, H. M. Chen, C. M. Li, T. Zhang, B. Liu, *Nat. Energy.* **2018**, *3*, 140.
[27] Y. G. Li, Z. S. Wu, P. F. Lu, X. Wang, W. Liu, Z. B. Liu, J. G. Ma, W. C. Ren, Z. Jiang, X. H. Bao, *Adv. Sci.* **2020**, *7*, 1903089.
[28] X. Zhang, Y. Wang, M. Gu, M. Y. Wang, Z. S. Zhang, W. Y. Pan, Z. Jiang, H. Z. Zheng, M. Lucero, H. L. Wang, G. E. Sterbinsky, Q. Ma, Y.-G. Wang, Z. X. Feng, J. Li, H. J. Dai, Y. Y. Liang, *Nat. Energy* **2020**, *5*, 684.
[29] Zheng, M. Lucero , H. L. Wang, G. E. Sterbinsky, Q. Ma, Y. G. Wang, Z. X. Feng, J. Li, H. J. Dai, Y. Y. Liang, *Nat. Energy* **2020**, *5*, 684.
[30] Y Hua, Y Shim, J Oh, S Park, S Park, Y Ishii, *Chem. Mater.* **2017**, *29*, 5080.
[31] Y. Hou, H. Guan, J. Yu, S. Cao, *Appl. Surf. Sci.* **2021**, *563*, 150310.
[32] Y. Okada, K. Chiba, *Chem. Rev.* **2018**, *118*, 4592.
[33] X. Li, J. G. Yu, M. Jaroniec, X. B. Chen, *Chem. Rev.* **2019**, *119*, 3962.
[34] Y. Du, H. Sheng, D. Astruc, M. Zhu, *Chem. Rev.* **2020**, *120*, 526.
[35] a) Y. O. Wang, X. Liu, X. Y. Han, R Godin, J. L. Chen, W. Z. Zhou, C. R. Jiang, J. F. Thompson, K. B. Mustafa, S. A. Shevlin, J. R. Durrant,

Z. X. Guo, J. W. Tang, *Nat. Commun.* **2020**, *20*, 2954; b) H. Kasap, C. A. Caputo, B. C. M. Martindale, R. Godin, V. W.-H. Lau, B. V. Lotsch, J. R. Durrant, E. Reisner, *J. Am. Chem. Soc.* **2016**, *138*, 9183.

[36] F. Guzman, S. S. C. Chuang, C. Yang, *Ind. Eng. Chem. Res.* **2013**, *52*, 61.

[37] A. M. Turek, I. E. Wachs, *J. Phys. Chem.* **1992**, *96*, 5000.

[38] J. W. Fu, K. X. Jiang, X. Q. Qiu, J. G. Yu, M. Liu, *Mater. Today* **2020**, *222*, 2432019.

[39] a) Z. J. Zhao, R. Mu, X. Wang, J. Gong, *Langmuir* **2017**, *33*, 8700; b) J. Szanyi, J. H. Kwak, *Phys. Chem. Chem. Phys.* **2014**, *16*, 15117.